Coherent spectral hole burning and qubit isolation by stimulated Raman adiabatic passage

Kamanasish Debnath,* Alexander Holm Kiilerich, Albert Benseny, and Klaus Mølmer
Department of Physics and Astronomy, Aarhus University, Ny Munkegade 120, DK-8000 Aarhus C, Denmark

(Received 28 March 2019; published 9 August 2019)

We describe how stimulated Raman adiabatic passage (STIRAP) can be applied to create spectral holes in an inhomogeneously broadened system. Due to the robustness of STIRAP, our proposal guarantees a high flexibility and accuracy, and at variance with traditional spectral hole burning techniques, it may require substantially fewer time resources since it does not rely upon the spontaneous decay of an intermediate excited state. We investigate the effects on the scheme of dephasing and dissipation as well as of unintentional driving of undesired transitions due to a finite splitting of the initial and target states. Finally, we show that the pulses can be reversed to create narrow absorption structures inside a broad spectral hole, which can be used as qubits for precise quantum operations on inhomogeneously broadened few-level systems.

DOI: 10.1103/PhysRevA.100.023813

I. INTRODUCTION

Within the last decade, we have seen a surge of interest in utilizing solid-state dopants like rare earth ions in crystals [1–4], nitrogen vacancy centers in nanodiamonds [5,6], and quantum dots in nanoscale semiconductors [7] for quantum operations. Experimentally, there has been significant progress, leading to single-photon sources [8], quantum memories [9], individual addressing of ions [5], observation of ultraslow group velocities of light [10], and much more. However, due to their complex structure and high density, all of these systems suffer from vast intrinsic inhomogeneous broadening [11–13]. The broadening is predominantly observed in the excited state since it interacts strongly with the surrounding crystal medium, which leads to a shift in the transition frequencies.

One well-known method to combat this inhomogeneous broadening is to employ spectral hole burning [14,15]. This is usually carried out by illuminating monochromatic (laser) light on the sample and sweeping the frequency across a range where the hole is desired. This excites near-resonant ions from the ground state to an excited state. A subsequent decay to a different ground state, not coupled by the laser, then leads to a hole in the spectrum around the chosen frequencies. This scheme is time-consuming, operating on a time scale defined by the lifetime of the excited state.

In this paper, we propose to utilize stimulated Raman adiabatic passage (STIRAP) [16,17] to create spectral holes and to establish isolated peaks in an inhomogeneously broadened absorption spectrum of dopant ions in a crystal, as illustrated in Figs. 1(a)–1(c). STIRAP constitutes a highly efficient technique to transfer population between internal levels of an ion or a molecule without populating the intermediate levels of the Raman transition. It is robust to variations in the applied laser fields and flexible in choosing the target level, and as long as the adiabaticity condition is fulfilled, it yields high fidelities [18]. STIRAP has been realized in a diverse range of settings such as trapped ions [19,20], chiral molecules [21], rare-earth-doped crystals [22–24], and even quantum computations [25,26]. For detailed reviews of this method see [18] and [27].

We consider an ensemble of Λ-type systems [see Fig. 1(d)] with a broad, inhomogeneous distribution [see Fig. 1(a)] of the transition frequencies to the excited state $|2\rangle$. In our scheme, spectral hole burning is achieved by adiabatically transferring the population from state $|1\rangle$ to state $|3\rangle$ for those ions with resonance frequencies around a predefined frequency ω_{target}. Despite the robustness of STIRAP against parameter variations, the population transfer fidelity drops if the detuning [Δ in Fig. 1(d)] is too large. We show that this defines a sharp cutoff at $\omega_{\text{target}} \pm \delta_\omega/2$, yielding a spectral hole with well-defined edges where, as illustrated in Fig. 1(b), every ion has been transferred to $|3\rangle$. The width δ_ω of this spectral hole can be tuned by the pulse parameters, and under ideal conditions one can engineer a spectral hole with a completely flat base.

In addition to coherent spectral hole burning, our protocol offers the possibility of *unburning* a part of the hole by adding a second set of reversed pulses with different parameters, thereby preparing a group of emitters which absorb light within a narrow frequency interval inside the wider spectral hole, as illustrated in Fig. 1(c). Such a reversed STIRAP (rSTIRAP) protocol can be used to isolate well-defined ions which may serve as qubits within a broad ensemble. This can be done at multiple frequency locations to create several qubits which, if geometrically located close to each other, experience dipole-dipole interactions that can facilitate the implementation of controlled-NOT gates [28]. Such an architecture will ultimately pave the way towards scalable quantum computing schemes relying on inhomogeneously broadened ensembles of quantum systems [29,30].

The paper is organized as follows. We start by presenting a generalized three-level model with a brief description of STIRAP in Sec. II. In Sec. III, we discuss the hole burning protocol and study the parameters that determine the shape

*kamanasish.debnath@phys.au.dk

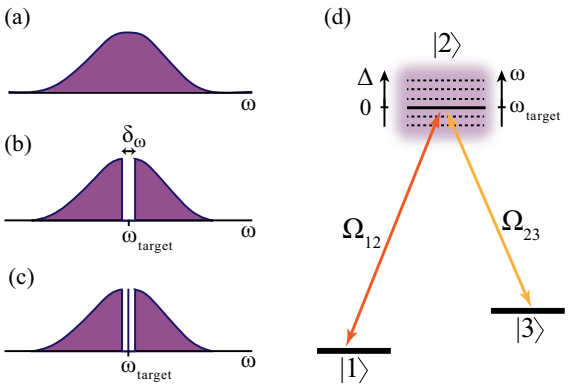

FIG. 1. Schematic of an idealized hole burning process using STIRAP. (a) Absorption profile of the $|1\rangle \leftrightarrow |2\rangle$ transition. (b) Spectral hole of width δ_ω around the central frequency ω_{target} after application of STIRAP. (c) Isolated (qubit) structure inside the spectral hole. (d) Level diagram and couplings commonly used in STIRAP. Dotted lines represent the excited state $|2\rangle$ for different ions, and the inhomogeneous broadening is illustrated by the shaded region. The bold line represents ions for which the pulses are resonant, i.e., for which $E_2 - E_1 = \hbar\omega_{\text{target}}$.

and width of the spectral hole. Furthermore, we evaluate the influence of decoherence channels, off-resonant cross coupling, and two-photon detuning on our scheme. Then, in Sec. IV, we introduce and characterize the reversed STIRAP process, which returns the population to $|1\rangle$ for a selected frequency range. Finally, we conclude with an outlook in Sec. V.

II. PHYSICAL SYSTEM

We consider a collection of three-level ions in a Λ configuration [Fig. 1(d)] which suffer from intrinsic inhomogeneous broadening as shown by the schematic of the absorption spectra of its $|1\rangle \leftrightarrow |2\rangle$ transition in Fig. 1(a). This can be any inhomogeneous system, for example, a given species of rare earth ion doped in a host crystal like Eu^{3+} ions in Y_2O_3 [1] or Y_2SiO_5 [3].

A. Three-level model

The two transitions $|1\rangle \leftrightarrow |2\rangle$ and $|2\rangle \leftrightarrow |3\rangle$ are driven at (time-dependent) Rabi frequencies $\Omega_{12}(t)$ and $\Omega_{23}(t)$. We drive the $|1\rangle \leftrightarrow |2\rangle$ transition at frequency ω_{target} (around which the spectral hole is desired) and assume the two-photon resonance condition, which fixes the driving frequency of the $|2\rangle \leftrightarrow |3\rangle$ transition. Due to the inhomogeneous broadening, each ion perceives a different detuning $\Delta_i = \omega_{\text{target}} - \omega_{12}^{(i)}$, where $\omega_{12}^{(i)}$ is the resonance frequency of the $|1\rangle \leftrightarrow |2\rangle$ transition of the ith ion. For simplicity of notation we omit the index on Δ_i below. Assuming the ions to be noninteracting, they each evolve independently according to a Hamiltonian ($\hbar = 1$),

$$H = \frac{\Omega_{12}(t)}{2}(|1\rangle\langle 2| + |2\rangle\langle 1|) + \frac{\Omega_{23}(t)}{2}(|2\rangle\langle 3| + |3\rangle\langle 2|) + \Delta|2\rangle\langle 2|. \quad (1)$$

In realistic settings, the excited state $|2\rangle$ has a finite lifetime and the ensemble suffers from dephasing due to crystal imperfections and stray magnetic fields. To assess the effects of such mechanisms on our proposal, we describe the evolution of our system by a Lindblad master equation,

$$\dot{\rho} = -i[H, \rho] + \gamma_{21}\mathcal{D}[|1\rangle\langle 2|]\rho + \gamma_{23}\mathcal{D}[|3\rangle\langle 2|]\rho + \Gamma\mathcal{D}[|2\rangle\langle 2| - |1\rangle\langle 1| - |3\rangle\langle 3|]\rho, \quad (2)$$

where we apply the superoperator $\mathcal{D}[\hat{\mathcal{O}}]\rho = \hat{\mathcal{O}}\rho\hat{\mathcal{O}}^\dagger - \frac{1}{2}\{\hat{\mathcal{O}}^\dagger\hat{\mathcal{O}}, \rho\}$ to describe spontaneous decay at rates γ_{21} and γ_{23} in the two optical transitions and dephasing at a rate Γ of the excited state relative to the two ground states.

B. STIRAP scheme

Hamiltonian (1) has one zero eigenvalue ($\varepsilon_0 = 0$), with corresponding eigenstate

$$|D\rangle = \cos\theta|1\rangle - \sin\theta|3\rangle. \quad (3)$$

The other eigenvalues are

$$\varepsilon_\pm = \tfrac{1}{2}\left(\Delta \pm \sqrt{\Delta^2 + \Omega_{\text{rs}}^2}\right) \quad (4)$$

and their corresponding eigenstates are

$$|+\rangle = \sin\theta\sin\phi|1\rangle + \cos\phi|2\rangle + \cos\theta\sin\phi|3\rangle, \quad (5)$$

$$|-\rangle = \sin\theta\cos\phi|1\rangle - \sin\phi|2\rangle + \cos\theta\cos\phi|3\rangle, \quad (6)$$

where

$$\tan\theta = \frac{\Omega_{12}}{\Omega_{23}}, \quad \tan 2\phi = \frac{\Omega_{\text{rms}}}{\Delta}, \quad (7)$$

with

$$\Omega_{\text{rms}} = \sqrt{\Omega_{12}^2 + \Omega_{23}^2}. \quad (8)$$

Clearly, $|D\rangle$ is a nonradiative dark state since it involves only the ground states $|1\rangle$ and $|3\rangle$ with a mixing angle θ, which depends on the two Rabi frequencies. The idea in STIRAP is to adiabatically follow this dark state while varying θ between $\theta = 0$ ($\Omega_{23} \gg \Omega_{12}$, $|D\rangle = |1\rangle$) and $\theta = \pi/2$ ($\Omega_{23} \ll \Omega_{12}$, $|D\rangle = -|3\rangle$). This will effectively transfer all the populations from $|1\rangle$ to $|3\rangle$. The introduction of a time delay $\tau > 0$ between the pulses ensures that the Ω_{23} pulse arrives before the Ω_{12} pulse. This constitutes the core mechanism in STIRAP; the first pulse opens an energy gap in the spectrum, allowing an adiabatic transfer when the second pulse arrives.

The basic requirement is thus that the two pulses overlap while the mixing angle θ is varied. However, as long as the adiabaticity condition is satisfied (see below), the exact shape of the pulses is immaterial. Hence, for simplicity, we consider Gaussian pulses with identical strengths $\Omega_{\max}$ and widths σ, as shown in Fig. 2(a):

$$\Omega_{12}(t) = \Omega_{\max}\exp\left(-\frac{(t - \tau/2)^2}{2\sigma^2}\right), \quad (9)$$

$$\Omega_{23}(t) = \Omega_{\max}\exp\left(-\frac{(t + \tau/2)^2}{2\sigma^2}\right). \quad (10)$$

In the discussion above, we have assumed that the system is initialized in state $|1\rangle$. We note that any initial population in $|3\rangle$ makes STIRAP ineffective. Hence a mandatory

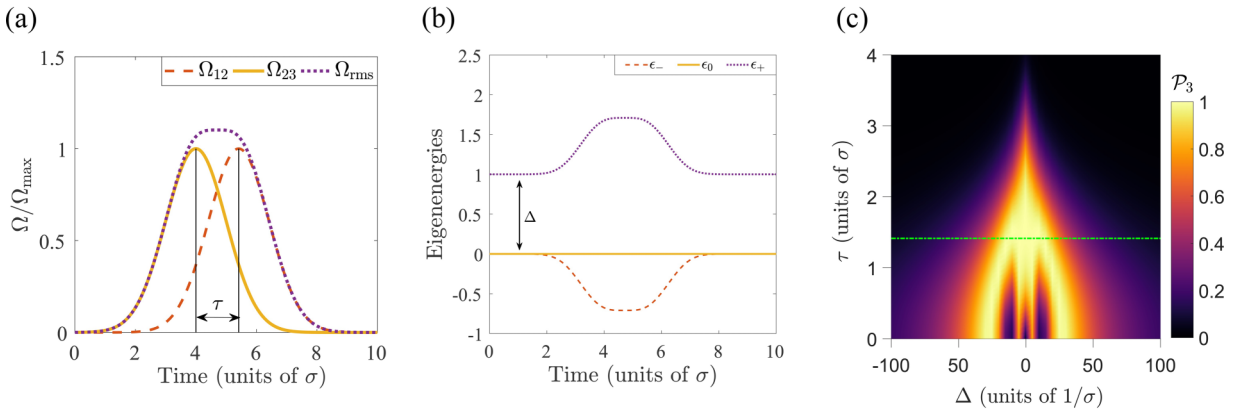

FIG. 2. STIRAP protocol. (a) Rabi frequencies during the protocol, with the delay τ indicated. (b) Spectrum of the Hamiltonian for positive detuning Δ during the protocol. (c) Final population $\mathcal{P}_3$ in state $|3\rangle$ as a function of the detuning Δ and pulse delay τ. The chosen (optimal) time delay $\tau = \sqrt{2}\sigma$, used throughout the article, is indicated by the dot-dashed green line. Results are shown for $\Omega_{\rm max} = 10\sigma^{-1}$ and $\gamma_{21} = \gamma_{23} = \Gamma = 0$.

requirement for our proposal is that the two stable ground states $|1\rangle$ and $|3\rangle$ are sufficiently separated to avoid any thermal excitations at equilibrium. While this may pose a problem in some settings (e.g., for systems with microwave ground-state splitting), systems with ground-state separation in the optical regime fulfill the requirement. For instance, our proposal may be implemented with Eu^{3+} ions doped in Y_2O_3 (Y_2SiO_5), using the hyperfine states $^7F_0$ and $^7F_2$ ($^7F_1$) as the two ground states $|1\rangle$ and $|2\rangle$ and $^5D_0$ as the intermediate state $|3\rangle$ [1,31]. With a Y_2O_3 crystal as the host medium, this entails a ground-state separation of 3×10^{13} Hz, implying a thermal excitation of less than 0.8% at room temperature. In a Y_2SiO_5 crystal, the ground-state splitting is smaller, 3×10^{12} Hz, and consequently, at room temperature the excitation is higher ($\approx$38%). However, at cryogenic temperatures of 4 K, state $|3\rangle$ is void of any excitations.

As a technical remark, we mention that, due to quadrupole interaction, the hyperfine $^7F_0$ level of doped Eu^{3+} ions experiences a splitting in the 10- to 100-MHz regime. To transfer ions at transition frequency $\omega_{\rm target}$ to the excited states out of all the quadrupole split $^7F_0$ levels μ therefore requires the application of STIRAP pulses with three frequencies ω_μ around $\omega_{\rm target}$, ensuring two-photon resonance towards different $^7F_2$ ($^7F_1$) sublevels. Note that while a three-level structure with two of the sublevels of the $^7F_0$ state is widely used for quantum memories [32], our proposal would not apply between these states as they are both populated at thermal equilibrium.

C. Adiabaticity and optimal time delay

In order to ensure an adiabatic transfer, the local adiabaticity condition must hold throughout the entire process. Namely,

$$|\varepsilon_0 - \varepsilon_\pm| \gg |\langle \pm|\dot{D}\rangle|, \tag{11}$$

which, in the absence of single-photon detuning ($\Delta = 0$), becomes $\Omega_{\rm rms} \gg |\dot{\theta}|$ [18]. This condition guarantees that there are no diabatic transitions out of the dark state $|D\rangle$ and can be fulfilled by a sufficiently slow process (having a slow rate of change of θ) or by a large enough gap (higher Rabi frequencies in $\Omega_{\rm rms}$).

In the next section we see how the presence of detuning due to inhomogeneity affects this condition, as we are interested in engineering a protocol which attains adiabaticity for a tunable range of frequencies δ_ω around $\omega_{\rm target}$ ($\Delta = 0$). We take the amplitude $\Omega_{\rm max}$ of the pulses as our main control parameter and, in the following, determine an optimal value of the time delay τ between pulses.

We simulate [33] the STIRAP process by considering the ions to be initially in $|1\rangle$ and apply the pulses shown in Fig. 2(a). The eigenvalues of the Hamiltonian in the presence of single-photon detuning Δ are plotted in Fig. 2(b). The final population $\mathcal{P}_3$ in $|3\rangle$ is shown in Fig. 2(c) as a function of the single-photon detuning Δ and pulse delay τ. For $\tau \ll \sigma$, both pulses are switched on almost simultaneously and both $|1\rangle$ and $|3\rangle$ are coupled to $|2\rangle$. This leads to Rabi oscillations between the different states, leaving population in the excited state at the final time. However, for certain values of the detuning (around $|\Delta| \simeq 25\sigma^{-1}$), perfect transfer into $|3\rangle$ is achieved. These points represent two-photon resonant Raman processes and unlike the STIRAP process, they are highly dependent on the Rabi frequencies and detuning. For $\tau \gg \sigma$, the process breaks down due to the complete temporal separation of the two pulses. The first pulse (Ω_{23}) has no effect since all the population is in $|1\rangle$ while it is on, and the second pulse leads simply to Rabi oscillations between $|1\rangle$ and $|2\rangle$. Between these extreme limits, however, there is a regime where STIRAP works perfectly. We fix $\tau = \sqrt{2}\sigma$, indicated by the dot-dashed green line in Fig. 2(c), which has been found to be an optimal value for the delay in similar studies [34].

In a related experiment [24], the efficiency of STIRAP is studied in a spectral hole (burned using conventional techniques) in a rare-earth-ion-doped crystal. They study the effects of varying $\Omega_{\rm max}$, Δ, and τ separately on the efficiency of the STIRAP but do not explore the possibility of applying the robustness of STIRAP to a well-defined range of frequencies Δ in a hole burning technique.

III. HOLE BURNING

We now describe how STIRAP can be used for hole burning in an inhomogeneously broadened sample. We initially

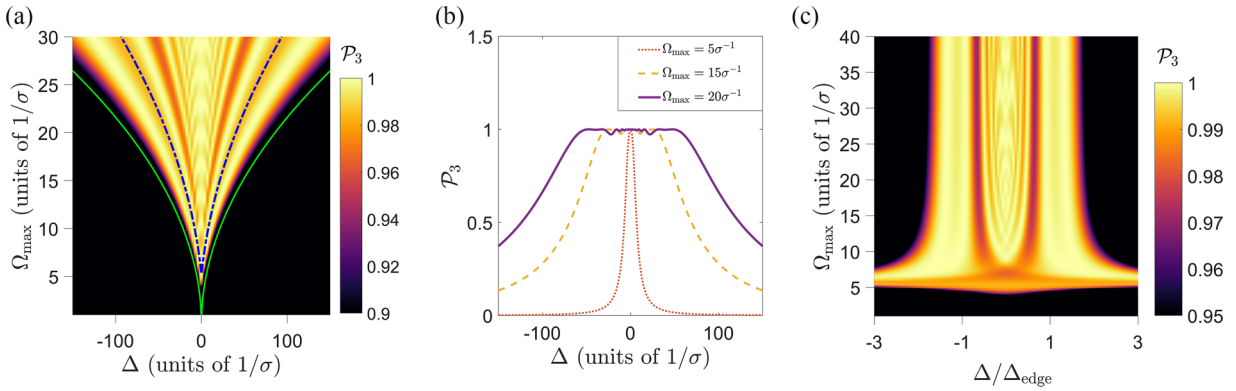

FIG. 3. Spectral hole burning. (a) $\mathcal{P}_3$ as a function of $\Omega_{\max}$ and detuning Δ. The dot-dashed blue line corresponds to $\pm\Delta_{\text{edge}}$ defined in Eq. (14). The bold green line corresponds to $\pm\Omega_{\text{rms}}^2/16\dot{\theta}$. (b) Spectral hole profile ($\mathcal{P}_3$) as a function of Δ for selected values of $\Omega_{\max}$. (c) $\mathcal{P}_3$ as a function of $\Omega_{\max}$ and detuning normalized to Δ_{edge}.

neglect the effects of dephasing and decay [$\gamma_{21} = \gamma_{23} = \Gamma = 0$ in the master equation (2)] but we discuss their implications for our results in Sec. III B.

A. Spectral hole profile

Figure 3(a) shows $\mathcal{P}_3$ after the STIRAP pulses as a function of Δ and $\Omega_{\max}$. We note that for weak pulses, STIRAP fails and only ions with $\Delta \simeq 0$ are transferred to state $|3\rangle$. However, as the strength of the pulses increases, the protocol becomes robust over a wider range of detunings, and the width δ_ω of the spectral hole increases. This is due to a growing energy gap between the dark state and the relevant bright state [see Eqs. (4) and our discussion below].

The spectral profile of the hole is shown in Fig. 3(b) for different values of $\Omega_{\max}$. From these plots, it is evident that while small oscillations appear in the base of the spectral hole, with higher values of $\Omega_{\max}$ one can achieve a spectral hole with a fairly flat base and sharply defined edges beyond which the population in $|3\rangle$ decreases to 0.

It is noteworthy that our simulations reveal that at the end of the transfer, the excited state $|2\rangle$ is not populated (all the population is in either state $|1\rangle$ or state $|3\rangle$) for any value of Δ considered in Fig. 3. For small Δ, this is guaranteed by the robust adiabatic following of the dark state, (3), while for large Δ it is due to the decoupling of the excited state from the two ground states.

We can address the width of the spectral hole by considering the effects of the single-photon detuning Δ on the adiabaticity condition. In the presence of a finite Δ, one of the bright states ($|+\rangle$ for $\Delta > 0$ and $|-\rangle$ for $\Delta < 0$) decouples from the dark state $|D\rangle$ with an energy gap larger than Δ. Therefore, it is sufficient to consider only the adiabaticity condition involving the other eigenstate. We focus our discussion on the case where $\Delta > 0$, study the coupling with $|-\rangle$, and note that the reverse situation ($\Delta < 0$, coupling to $|+\rangle$) produces the expected symmetrical results. The STIRAP adiabaticity condition, (11), yields approximately $|\Delta| \ll \Omega_{\text{rms}}^2/8\dot{\theta}$, which already gives the scaling of the width with the pulse parameters. As shown by the green line in Fig. 3(a), defining the edge of the hole at $\pm\Omega_{\text{rms}}^2/16\dot{\theta}$ fits the numerical data with good agreement.

We may apply a simple model which captures the essential features of the STIRAP transition and allows analytic insight regarding the width and detailed profile of the spectral hole and its dependence on the pulse parameters. The model assumes that $\Omega_{\text{rms}}(t)$ and $\phi(t)$ are constant while the mixing angle $\theta(t) = \pi t/2T$ varies linearly between 0 and $\pi/2$ during a time T. This approximates well the Gaussian pulses in Eqs. (9) and (10) in the time interval between their maxima where the main part of the STIRAP process happens.

In the absence of dephasing and decay, a perturbative treatment yields the probability of a nonadiabatic transition out of the dark state [35],

$$P_{\text{trans}} \simeq \frac{\left|\int_0^T \langle -|\dot{D}\rangle \exp\left[-i\int_0^t \delta_\epsilon\, dt'\right] dt\right|^2}{\left|\int_0^T \langle -|\dot{D}\rangle dt\right|^2}. \tag{12}$$

Under the above conditions, both the energy gap $\delta_\epsilon \equiv (\varepsilon_0 - \varepsilon_-)$ and the nonadiabatic coupling $\langle -|\dot{D}\rangle$ remain constant, and we obtain an analytical estimate for the final population of state $|3\rangle$,

$$\mathcal{P}_3 = 1 - P_{\text{trans}} = 1 - \text{sinc}^2\left(\frac{\pi\delta_\epsilon}{4\dot{\theta}}\right), \tag{13}$$

where $\text{sinc}(x) = \sin(x)/x$. Note that $\delta_\epsilon = (\sqrt{\Delta^2 + \Omega_{\text{rs}}^2} - \Delta)/2$ decreases monotonically as Δ increases. The edge of the spectral hole is defined by the first 0 of the sinc function, which occurs when $\pi\delta_\epsilon/4\dot{\theta} = \pi$, yielding

$$\Delta_{\text{edge}} = \frac{\Omega_{\text{rms}}^2}{16\dot{\theta}} - 4\dot{\theta}, \tag{14}$$

where Ω_{rms} is defined in Eq. (8), and a corresponding hole width of $\delta_\omega = 2\Delta_{\text{edge}}$. For $|\Delta| < \Delta_{\text{edge}}$, $\mathcal{P}_3$ is close to 1, giving a flat plateau for the spectral hole [$\text{sinc}^2(x) < 0.05$ for $x > \pi$]. For $|\Delta| > \Delta_{\text{edge}}$, $\mathcal{P}_3$ rapidly decreases, and for large Δ, Eq. (13) can be approximated as $\mathcal{P}_3 \simeq (\pi^2\Omega_0^4/768\dot{\theta}^2\Delta^2) + O[1/\Delta^4]$.

In order to apply this expression to the Gaussian pulses, we approximate the parameter values by those at the instant between the two pulses [i.e., Eqs. (9) and (10) at $t = 0$], giving $\Omega_{\text{rms}} \simeq \sqrt{2}e^{-\tau^2/8\sigma^2}\Omega_{\max}$ and $\dot{\theta} \simeq \tau/2\sigma^2$. With these approximations, Δ_{edge} is shown by the dot-dashed blue line

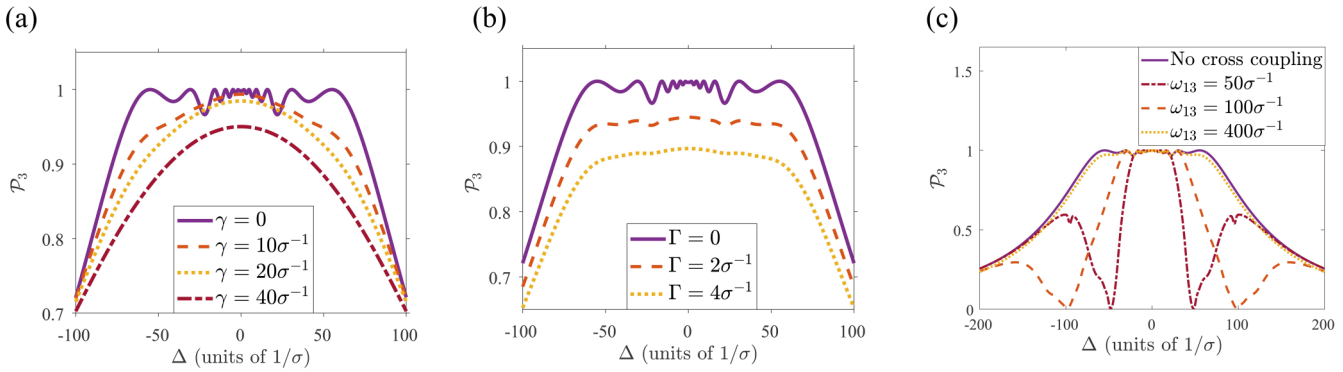

FIG. 4. Effects of decay and dephasing. Spectral hole profile ($\mathcal{P}_3$) as a function of Δ for different values of (a) the excited-state decay rates $\gamma_{21} = \gamma_{23} = \gamma$ and (b) the excited-state dephasing rate Γ. Results are shown for $\Omega_{\max} = 20\sigma^{-1}$. (c) $\mathcal{P}_3$ for different values of the splitting ω_{13} between stable state $|1\rangle$ and stable state $|3\rangle$. The solid curve assumes that each laser couples only to the desired transition in the ions. Results are shown for $\Omega_{\max} = 20\sigma^{-1}$ and $\Gamma = \gamma_{21} = \gamma_{23} = 0$.

in Fig. 3(a), which fits the numerical data with reasonable agreement.

We can also use Eq. (13) to understand the structure of the base of the hole as shown in Fig. 3(b). The oscillatory structure is defined by the tail of the sinc function beyond its first 0. The maximum value of the argument is $\pi\Omega_{\rm rms}/8\dot{\theta}$ (at $\Delta = 0$), which dictates the number of oscillations and how flat the base appears (how far out the sinc tail it starts). Figure 3(c) shows $\mathcal{P}_3$ as a function of $\Delta/\Delta_{\rm edge}$ and the pulse intensity $\Omega_{\max}$. This allows us to see the generality of this simple model in predicting the cutof and to visualize the structures of the spectral hole with its increasing flatness as $\Omega_{\max}$ increases.

B. Effects of decay and dephasing

While the results presented above signify that under ideal conditions STIRAP allows well-defined and broad holes to be burned in an inhomogeneous profile, any realistic setup will experience experimental or fundamental limitations. In the following, we study the effects of decay and dephasing on the hole burning process.

We show in Fig. 4(a) the profile of the spectral hole for different decay rates of the excited state ($\gamma_{21} = \gamma_{23} \equiv \gamma \geqslant 0$). We find that as the rate of decay increases, the flat profile of the spectral hole is lost. Moreover, for very large values of γ even the high fidelity at resonance is lost.

In Fig. 4(b), it is shown that while our protocol is robust in the absence of nonradiative dephasing ($\Gamma \geqslant 0$) of the excited state, as the dephasing increases, the final population $\mathcal{P}_3$ in state $|3\rangle$ starts decreasing. At variance with the effects of decay, however, the flatness of the hole is preserved as the fidelity decreases globally.

Our results thus show that for systems with large environmental couplings, the STIRAP hole burning protocol becomes inefficient. However, realistic dephasing and decay rates are typically much lower than the values considered in Fig. 4 [1], ensuring good performance for ions in quantum information processing tasks.

C. Effects of off-resonant cross coupling

Thus far we have assumed that each laser couples only to the desired transition in the ions. For some ions, however, the detuning may be comparable to the splitting between the stable states ($|\Delta| \simeq \omega_{13}$), and one of the STIRAP laser pulses may unintentionally excite the wrong transitions. In other words, due to inhomogeneous broadening, Ω_{12} (Ω_{23}) may be resonant with the $|3\rangle \leftrightarrow |2\rangle$ ($|1\rangle \leftrightarrow |2\rangle$) transition for particular groups of ions, as described by the contributions to the Hamiltonian,

$$H_{\rm cc} = \frac{\Omega_{23}(t)}{2}(|1\rangle\langle 2|e^{-i\omega_{13}t} + |2\rangle\langle 1|e^{i\omega_{13}t}) + \frac{\Omega_{12}(t)}{2}(|3\rangle\langle 2|e^{i\omega_{13}t} + |2\rangle\langle 3|e^{-i\omega_{13}t}), \quad (15)$$

that are disregarded in Eq. (1).

In Fig. 4(c) it is shown that as long as the level splitting is larger than the desired spectral hole (cf. the curve for $\omega_{13} = 400\sigma^{-1}$), the effects of this cross coupling are insignificant in the intended frequency range. For smaller level splittings, however, the hole width is reduced, as STIRAP becomes completely ineffective and yields no final population in $|3\rangle$ for the resonances $\Delta = \pm\omega_{13}$ (cf. the dips for the $\omega_{13} = 50\sigma^{-1}$ and $100\sigma^{-1}$ curves). It is thus evident that the energy splitting imposes an upper bound $\delta_\omega \lesssim 2\omega_{13}$ on the width of the spectral hole. Note that a similar restriction applies for conventional hole burning.

D. Effects of two-photon detuning

As explained in Sec. II A, we have thus far assumed the two-photon resonance to be fulfilled. However, it is well known that STIRAP is very sensitive to a two-photon detuning δ as described by an additional contribution to the Hamiltonian [18],

$$H_\delta = \delta|3\rangle\langle 3|. \quad (16)$$

In what follows, we simulate the consequences of finite δ on the spectral hole. The results in Fig. 5 reveal that while larger values of δ have severe consequences, the hole burning scheme is unaffected by the two-photon detuning for $\delta \lesssim 0.1\sigma^{-1}$ (see inset). For instance, with $\sigma \approx 20$ μs and $\Omega_{\max} = 15\sigma^{-1} \approx 750$ kHz [24], this corresponds to $\delta \lesssim 5$ kHz, which is well within experimental feasibility with well-tuned lasers.

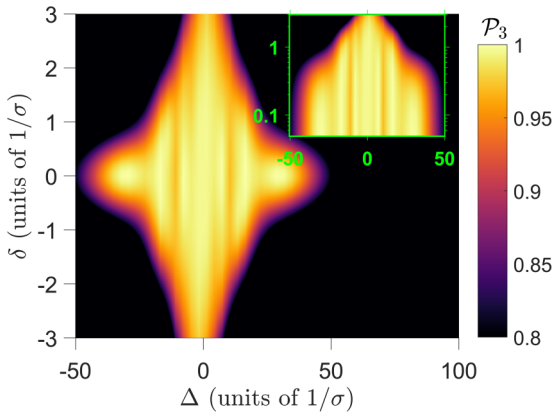

FIG. 5. Spectral hole profile ($\mathcal{P}_3$) for different values of the two-photon detuning δ and one-photon detuning Δ. Inset: The same data on a logarithmic scale for $\delta > 0$. Results are shown for $\Omega_{\max} = 15\sigma^{-1}$ and $\Gamma = \gamma_{21} = \gamma_{23} = 0$.

A more relevant concern is a finite broadening of the ground states, which would imply a two-photon detuning for some ions within the desired spectral hole. For the systems we have in mind and where our scheme will find relevance (e.g., rare earth ions doped in crystals), however, the broadening of the ground states is several orders of magnitude smaller than that of the excited state. For instance, in the spectroscopic study in Ref. [1], the $|2\rangle \leftrightarrow |3\rangle$ transition was used to determine the inhomogeneous broadening of state $|2\rangle$, which was feasible only because the broadening of the ground state is much smaller than that of the excited state. Considering a GHz-broadened excited state, the ground-state broadening is of the order of a few kHz and our protocol should operate perfectly.

IV. QUBIT ISOLATION

We have shown how STIRAP can be utilized to create spectral holes with a high fidelity. In this section, we propose to follow that process with a set of *reversed* STIRAP pulses of lower intensity in order to bring some atoms back into state $|1\rangle$ and create narrow-band peaked structures at target frequencies $\omega^{(n)}_{\text{target}}$ inside the burned hole. This can be used, for instance, in quantum information processing to effectively create one or multiple isolated qubits in an inhomogeneous sample [29,30].

A. Reversed STIRAP

Assuming ideal conditions, after the initial STIRAP pulses, all ions inside the spectral hole are in state $|3\rangle$. Therefore, a new set of reversed pulses [Ω_{12} acting before Ω_{23}, i.e., $\tau < 0$ in Eqs. (9) and (10)] will adiabatically bring a selected band of them back to state $|1\rangle$. As discussed in the previous section, the width of the band is tunable through the pulse intensity, and less intense pulses thus allow us to bring back a much narrower band of the spectrum. The set of STIRAP and rSTIRAP pulses in this process is depicted in Fig. 6(a), which also shows how the mixing angle $\theta(t)$ (dotted blue line) varies from 0 to $\pi/2$ for the STIRAP pulses, followed by its return to 0 during the rSTIRAP pulses.

Figure 6(b) shows how the strength of the second set of pulses, $\Omega^{(r)}_{\max}$, influences the final population in $|1\rangle$ for different values of Δ (after the hole has been created). It is shown that, in a similar manner as for the original hole burning, the strength of the rSTIRAP pulses can indeed be used to control the width of the *unburnt* frequency band. The figure shows also the limit on how narrow these peaks can be created, as dictated by the adiabaticity condition: if $\Omega^{(r)}_{\max}$ is too small, rSTIRAP fails for *all* values of Δ, resulting in a peak with less than unit population in $|1\rangle$.

B. Isolation profiles

We show in Fig. 6(c) the profile of a narrow isolated peak inside a broad spectral hole, signifying that the combination of STIRAP and rSTIRAP processes can be successfully employed to create well-defined systems within a broad inhomogeneous ensemble. The wiggles in the spectral hole (see Fig. 3) can cause a small loss of fidelity of the imprinted structures around the desired qubit. However, for multiqubit quantum computing protocols [30], the isolated emitters will dominate over the background.

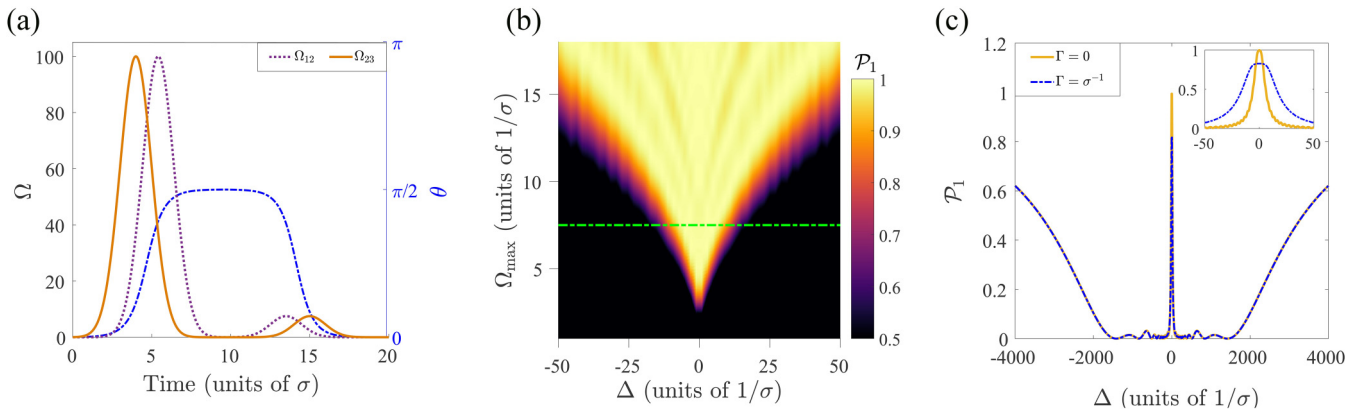

FIG. 6. Qubit isolation around a single target frequency $\omega^{(n)}_{\text{target}}$ coinciding with the center of the spectral hole. (a) Rabi frequencies $\Omega_{12}(t)$ and $\Omega_{23}(t)$ and mixing angle $\theta(t)$ during the combined STIRAP and rSTIRAP protocols. (b) Final population $\mathcal{P}_1$ in state $|1\rangle$ as a function of the detuning and pulse amplitude of rSTIRAP. (c) Final population $\mathcal{P}_1$ in state $|1\rangle$ in the presence and absence of dephasing for the pulses shown in (a). Inset: Zoom-in on the central structure. Results are shown for $\gamma_{21} = \gamma_{23} = 0$.

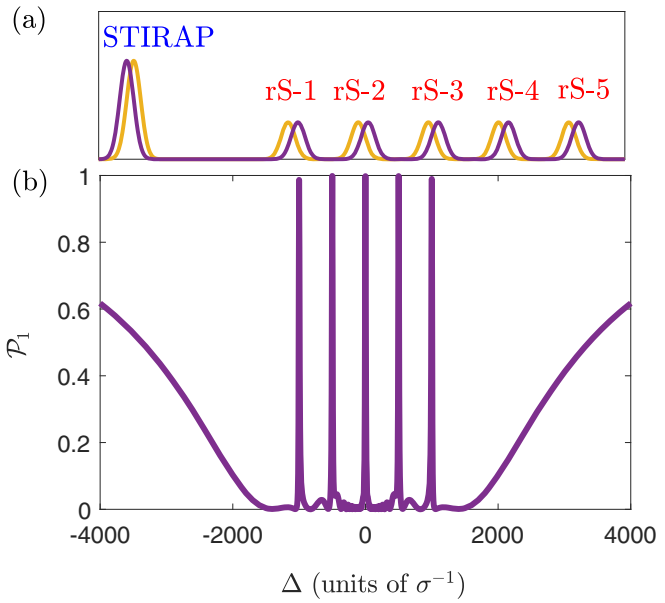

FIG. 7. Multiple isolated qubits. (a) Sketch of the STIRAP pulses and subsequent sets of rSTIRAP pulses with five target frequencies, $\omega_{\text{target}}^{(n)} = \omega_{\text{target}} + n \times 500\sigma^{-1}$, with $n = -2,\ -1,\ 0,\ 1,\ 2$. (b) Final population $\mathcal{P}_1$ in state $|1\rangle$ after the train of pulses. Results are shown for $\Omega_{\text{max}} = 100\sigma^{-1}$, $\Omega_{\text{max}}^{(r)} = 5\sigma^{-1}$, $\gamma_{21} = \gamma_{23} = \Gamma = 0$.

It is possible to isolate multiple qubits inside the same broad spectral hole. We illustrate this in Fig. 7, where the sequential application of five sets of rSTIRAP pulses with different target frequencies $\omega_{\text{target}}^{(n)}$ yield five well-defined qubits inside the hole. While here we have assumed the serial application of the different rSTIRAP pulses, it should also be possible to create an atomic frequency comb [36,37], i.e., a number of equidistant isolated qubits, by simultaneously applying the rSTIRAP pulses with an optical frequency comb; see also Ref. [38] for a related proposal in a Doppler-broadened system.

V. OUTLOOK

In this paper, we have shown how STIRAP can be used for coherent spectral hole burning with a high fidelity and better control of the shape of the spectral hole. We derived an analytical expression that estimates the width of the hole as a function of the pulse intensity and emphasize how a hole with well-defined edges may be obtained due to the adiabaticity requirement in the STIRAP scheme. Moreover, we proposed to apply additional sets of weaker STIRAP pulses to isolate qubits inside the spectral hole. STIRAP is highly flexible in targeting any state and the entire process requires just two Gaussian pulses.

Our proposal is robust against variations in pulse parameters as long as the adiabaticity condition is fulfilled and against moderate decoherence in the excited state. For clarity of presentation, we have focused our attention on Gaussian pulses. However, in a future study it would be interesting to consider the possibilities offered by more complex pulse shapes which may deliver spectral holes with sharper edges and other desirable features.

The parameters considered in this paper are compatible with the state-of-the-art developments in the experimental domain. For instance, for Eu^{3+} ions doped in an Y_2O_3 crystal [1], the two stable states in our model may be the hyperfine states $^7F_0$ and $^7F_2$ with transition frequencies $\omega_{12} = 2\pi \times 5.167 \times 10^{14}$ Hz and $\omega_{23} = 2\pi \times 4.903 \times 10^{14}$ Hz to the excited state $^5D_0$. The excited state is known to have an inhomogeneous broadening of 22 GHz [1]. Assuming that one desires to create a spectral hole of width $\delta_\omega \approx 1$ MHz with isolated (qubit) structures a few kHz wide inside, the dephasing and decay rates of $\Gamma = 2\pi \times 0.785$ kHz and $\gamma = 2 \times \times 45$ kHz are low and will not severely affect the efficiency of STIRAP. In addition, the ground-state separation is of the order of $\omega_{13} \simeq 2\pi \times 0.3 \times 10^{14}$ Hz $\gg \delta_\omega$, implying that off-resonant cross coupling is negligible for these systems.

ACKNOWLEDGMENTS

We would like to thank Signe Seidelin and Bess Fang for discussions on possible candidate systems for our proposal. K.D. and K.M. were supported by the European Union's Horizon 2020 research and innovation program (Grant No. 712721, NanoQtech). A.H.K. and K.M. acknowledge support from the European Union FETFLAG program Grant No. 820391 (SQUARE). A.B. and K.M. were supported by the Villum Foundation.

[1] B. Casabone, J. Benedikter, T. Hümmer, F. Oehl, K. de O. Lima, T. W. Hänsch, A. Ferrier, P. Goldner, H. de Riedmatten, and D. Hunger, Cavity-enhanced spectroscopy of a few-ion ensemble in Eu^{3+}:Y_2O_3, New J. Phys. **20**, 095006 (2018).

[2] S. R. Hastings-Simon, M. Afzelius, J. Minář, M. U. Staudt, B. Lauritzen, H. de Riedmatten, N. Gisin, A. Amari, A. Walther, S. Kröll, E. Cavalli, and M. Bettinelli, Spectral hole-burning spectroscopy in Nd^{3+}:YVO_4, Phys. Rev. B **77**, 125111 (2008).

[3] O. Gobron, K. Jung, N. Galland, K. Predehl, R. L. Targat, A. Ferrier, P. Goldner, S. Seidelin, and Y. L. Coq, Dispersive heterodyne probing method for laser frequency stabilization based on spectral hole burning in rare-earth doped crystals, Opt. Express **25**, 15539 (2017).

[4] M. Mitsunaga, R. Yano, and N. Uesugi, Time- and frequency-domain hybrid optical memory: 1.6-kbit data storage in Eu^{3+}:Y_2SiO_5, Opt. Lett. **16**, 1890 (1991).

[5] H. Kaupp, T. Hümmer, M. Mader, B. Schlederer, J. Benedikter, P. Haeusser, H.-C. Chang, H. Fedder, T. W. Hänsch, and D. Hunger, Purcell-Enhanced Single-Photon Emission from Nitrogen-Vacancy Centers Coupled to a Tunable microcavity, Phys. Rev. Appl. **6**, 054010 (2016).

[6] J. R. Weber, W. F. Koehl, J. B. Varley, A. Janotti, B. B. Buckley, C. G. Van de Walle, and D. D. Awschalom, Quantum computing with defects, Proc. Natl. Acad. Sci. U.S.A. **107**, 8513 (2010).

[7] S.-W. Feng, C.-Y. Cheng, C.-Y. Wei, J.-H. Yang, Y.-R. Chen, Y.-W. Chuang, Y.-H. Fan, and C.-S. Chuu, Purification of Single

Photons from Room-Temperature Quantum Dots, Phys. Rev. Lett. **119**, 143601 (2017).

[8] C. Kurtsiefer, S. Mayer, P. Zarda, and H. Weinfurter, Stable Solid-State Source of Single Photons, Phys. Rev. Lett. **85**, 290 (2000).

[9] B. Julsgaard, C. Grezes, P. Bertet, and K. Mølmer, Quantum Memory for Microwave Photons in an Inhomogeneously Broadened Spin Ensemble, Phys. Rev. Lett. **110**, 250503 (2013).

[10] A. V. Turukhin, V. S. Sudarshanam, M. S. Shahriar, J. A. Musser, B. S. Ham, and P. R. Hemmer, Observation of Ultraslow and Stored Light Pulses in a Solid, Phys. Rev. Lett. **88**, 023602 (2001).

[11] A. O. Levchenko, V. V. Vasil'ev, S. A. Zibrov, A. S. Zibrov, A. V. Sivak, and I. V. Fedotov, Inhomogeneous broadening of optically detected magnetic resonance of the ensembles of nitrogen-vacancy centers in diamond by interstitial carbon atoms, Appl. Phys. Lett. **106**, 102402 (2015).

[12] R. L. Ahlefeldt, M. R. Hush, and M. J. Sellars, Ultranarrow Optical Inhomogeneous Linewidth in a Stoichiometric Rare-Earth Crystal, Phys. Rev. Lett. **117**, 250504 (2016).

[13] M. Nilsson, L. Rippe, S. Kröll, R. Klieber, and D. Suter, Hole-burning techniques for isolation and study of individual hyperfine transitions in inhomogeneously broadened solids demonstrated in Pr^{3+}:Y_2SiO_5, Phys. Rev. B **70**, 214116 (2004).

[14] K. Holliday, M. Croci, E. Vauthey, and U. P. Wild, Spectral hole burning and holography in an Y_2SiO_5:P^{3+} crystal, Phys. Rev. B **47**, 14741 (1993).

[15] K. Naoe, L. G. Zimin, and Y. Masumoto, Persistent spectral hole burning in semiconductor nanocrystals, Phys. Rev. B **50**, 18200 (1994).

[16] U. Gaubatz, P. Rudecki, S. Schiemann, and K. Bergmann, Population transfer between molecular vibrational levels by stimulated Raman scattering with partially overlapping laser fields. A new concept and experimental results, J. Chem. Phys. **92**, 5363 (1990).

[17] L. S. Goldner, C. Gerz, R. J. C. Spreeuw, S. L. Rolston, C. I. Westbrook, W. D. Phillips, P. Marte, and P. Zoller, Coherent transfer of photon momentum by adiabatic following in a dark state, Quantum Opt.: J. Eur. Opt. Soc. B **6**, 387 (1994).

[18] N. V. Vitanov, A. A. Rangelov, B. W. Shore, and K. Bergmann, Stimulated Raman adiabatic passage in physics, chemistry, and beyond, Rev. Mod. Phys. **89**, 015006 (2017).

[19] J. L Sørensen, D. Møller, T. Iversen, J. B. Thomsen, F. Jensen, P. Staanum, D. Voigt, and M. Drewsen, Efficient coherent internal state transfer in trapped ions using stimulated Raman adiabatic passage, New J. Phys. **8**, 261 (2006).

[20] F. Gebert, Y. Wan, F. Wolf, C. N. Angstmann, J. C. Berengut, and P. O. Schmidt, Precision Isotope Shift Measurements in Calcium Ions Using Quantum Logic Detection Schemes, Phys. Rev. Lett. **115**, 053003 (2015).

[21] S. Schiemann, A. Kuhn, S. Steuerwald, and K. Bergmann, Efficient Coherent Population Transfer in no Molecules Using Pulsed Lasers, Phys. Rev. Lett. **71**, 3637 (1993).

[22] J. Klein, F. Beil, and T. Halfmann, Robust Population Transfer by Stimulated Raman Adiabatic Passage in a Pr^{3+} Y_2SiO_5 Crystal, Phys. Rev. Lett. **99**, 113003 (2007).

[23] A. L. Alexander, R. Lauro, A. Louchet, T. Chanelière, and J. L. Le Gouët, Stimulated Raman adiabatic passage in Tm^{3+}:YAG, Phys. Rev. B **78**, 144407 (2008).

[24] J. Klein, F. Beil, and T. Halfmann, Experimental investigations of stimulated Raman adiabatic passage in a doped solid, Phys. Rev. A **78**, 033416 (2008).

[25] X. Lacour, N. Sangouard, S. Guérin, and H. R. Jauslin, Arbitrary state controlled-unitary gate by adiabatic passage, Phys. Rev. A **73**, 042321 (2006).

[26] I. I. Beterov, M. Saffman, E. A. Yakshina, V. P. Zhukov, D. B. Tretyakov, V. M. Entin, I. I. Ryabtsev, C. W. Mansell, C. MacCormick, S. Bergamini, and M. P. Fedoruk, Quantum gates in mesoscopic atomic ensembles based on adiabatic passage and Rydberg blockade, Phys. Rev. A **88**, 010303(R) (2013).

[27] K. Bergmann, N. V. Vitanov, and B. W. Shore, Perspective: Stimulated Raman adiabatic passage: The status after 25 years, J. Chem. Phys. **142**, 170901 (2015).

[28] I. Roos and K. Mølmer, Quantum computing with an inhomogeneously broadened ensemble of ions: Suppression of errors from detuning variations by specially adapted pulses and coherent population trapping, Phys. Rev. A **69**, 022321 (2004).

[29] J. H. Wesenberg, K. Mølmer, L. Rippe, and S. Kröll, Scalable designs for quantum computing with rare-earth-ion-doped crystals, Phys. Rev. A **75**, 012304 (2007).

[30] N. Ohlsson, R. K. Mohan, and S. Kröll, Quantum computer hardware based on rare-earth-ion-doped inorganic crystals, Opt. Commun. **201**, 71 (2002).

[31] J. H. Wesenberg, Quantum information processing in rare-earth-ion doped crystals, Ph.D. thesis, University of Aarhus, 2004.

[32] M. Zhong, M. P. Hedges, R. L. Ahlefeldt, J. G. Bartholomew, S. E. Beavan, S. M. Wittig, J. J. Longdell, and M. J. Sellars, Optically addressable nuclear spins in a solid with a six-hour coherence time, Nature **517**, 177 (2015).

[33] J. R. Johansson, P. D. Nation, and F. Nori, QuTiP 2: A Python framework for the dynamics of open quantum systems, Comput. Phys. Commun. **184**, 1234 (2013).

[34] K. Bergmann, H. Theuer, and B. W. Shore, Coherent population transfer among quantum states of atoms and molecules, Rev. Mod. Phys. **70**, 1003 (1998).

[35] A. Messiah, *Quantum Mechanics, Vol. II* (North-Holland, Amsterdam, 1961).

[36] M. Afzelius, C. Simon, H. de Riedmatten, and N. Gisin, Multimode quantum memory based on atomic frequency combs, Phys. Rev. A **79**, 052329 (2009).

[37] M. Afzelius, I. Usmani, A. Amari, B. Lauritzen, A. Walther, C. Simon, N. Sangouard, J. Minář, H. de Riedmatten, N. Gisin, and S. Kröll, Demonstration of Atomic Frequency Comb Memory for Light With Spin-Wave Storage, Phys. Rev. Lett. **104**, 040503 (2010).

[38] J. L. Rubio, D. Viscor, J. Mompart, and V. Ahufinger, Atomic-frequency-comb quantum memory via piecewise adiabatic passage, Phys. Rev. A **98**, 043834 (2018).